Malaysian Journal of Chemistry, 2025, Vol. 27(3), 115-125
(Special Issue: *2nd International Science and Technology Colloquium, i-COSTECH 2024*)

Poly(methyl methacrylate)/50% Epoxidized Natural Rubber-Based Electrolyte: The Effect of Rice Husk Ash Silica on the Structural and Electrical Properties

Siti Zulaikha Mohd Yusof[1], Siti Nurni Kamilla Abdullah[1], Nur Aisyah Abdul Rahman[1], Nabilah Akemal Muhd Zailani[1]*, Khuzaimah Nazir[1], Dalina Samsudin[1] and Zeyana Saif Mubarak Al Shukaili[2]

[1]Faculty of Applied Sciences, Universiti Teknologi MARA, Cawangan Perlis, Kampus Arau, 02600 Arau, Perlis, Malaysia

[2]Ministry of Education, Muscat, Sultanat Oman

*Corresponding author (email: nabilahakemal@uitm.edu.my)

The issues that related to low ionic conductivity (σ) of poly(methyl methacrylate) (PMMA) and epoxidized natural rubber (ENR 50) electrolyte system has been succesfully solved with the incorporation of plasticizers. Its mechanical strength is nonetheless diminished as a result of this. On the other hand, the insertion of filler improved the polymer electrolyte results for ionic conductivity and flexibility, while preserving its mechanical characteristics. In this work, the PMMA/ENR 50-based electrolyte system was supplemented with various amounts of silica filler made from rice husk ash (RHA) in weight percentages of 0.25, 0.5, 0.75, and 1.0 by solution casting. The precipitation technique efficiently extracted silica from RHA with a mean particle size of about 75.76 µm. The purity and structure of the silica were validated using energy-dispersive x-ray spectroscopy (EDX) and Fourier transform infrared spectroscopy (FTIR), respectively. The scanning electron microscopy (SEM) and x-ray diffraction (XRD) studies verify the amorphous nature of the silica. Flexible, free-standing, and homogenous films of silica-doped PMMA/ENR 50-based electrolyte were successfully prepared with the incorporation of up to 0.5 wt.% of silica with the highest σ of 1.37×10^{-3} S/cm. This was contributed by the interaction of polymer-filler as the amorphous phase of the system increased, as well as the interaction of salt-filler contributed to the existence of conducting pathway for new Li ion. The analysis from FTIR validated the interactions between polymer-salt-filler systems.

Keywords: Poly(methyl methacrylate); silica; rice husk ash; polymer electrolytes; epoxidized natural rubber

Received: September 2024; Accepted: November 2024

Nowadays, portable devices and electric transport both make substantial use of lithium-ion batteries because of their energy efficiency as well as environmental benefits [1]. However, despite their benefits, safety concerns remain a challenge. The use of liquid electrolytes in these batteries can cause issues like corrosion, leakage, and even explosions, limiting their future development. In this work, new polymer electrolyte system has been prepared in thin films form, which increase safety by minimizing the risk of internal shorting, gas formation, electrolyte leakage, and combustible product reactions on the electrode surface, as faced by liquid electrolyte [2].

Poly (methyl methacrylate) (PMMA), in thin film form, is extensively used in PE as a polymer host due to its stability towards electrode if compared to other polymers. PMMA owns C=O and -OCH_3 groups which will provide sites for ionic conduction [3]. However, commercial PMMA generally forms brittle films with weak adhesion to electrode surfaces, resulting in an "air gap" that decreases ionic conduction. In response to this issue, researchers implemented the polymer blending technique, which involves adding secondary polymers [4, 5]. Harun & Chan [6] reported that 50 % epoxidized natural rubber (ENR 50) possesses great impact resistance, good dimensional stability, low glass transition temperature (T_g), and significant stickiness. These properties allow it to create effective connection between the electrode and electrolyte layer in electrical devices. Moreover, research has shown that mixing natural polymers like ENR 50 with the synthetic polymers can increase the biodegradability of the polymer blend [7]. However, the phase separation issue has been a problem for polymer blends like PMMA/ENR50. This is because the films with phase separation exhibit coarse morphologies which will cause poor electrode-electrolyte contact and lowers the ionic conductivity of the system [8].

The incorporation of fillers (i.e., SiO_2, Al_2O_3, and TiO_2) into the system have been shown to prevent phase separation and enhance the homogeneity in PMMA/ENR 50 blends, increasing mechanical strength and ionic conductivity [9]. According to Basri et al.

†Paper presented at the 2nd International Science and Technology Colloquium (i-COSTECH 2024)

[4], the incorporation of high dielectric constant fillers into a polymeric system will improve its conductivity. The dumping of rice husk ash (RHA) will cause environmental threat to the surrounding as its production reached 20 million tons per year worldwide. This leads to the commercialization efforts of RHA. As RHA comprise around 85-90% amorphous silica [10], utilizing it as a filler will increase the conductivity and mechanical characteristics of PE while also promoting sustainability. The study done by Habep et al. [11] reported that the incorporation of alumina filler has successfully boosted the conductivity of the PMMA/ENR 50 system due to the improved amorphosity and the creation of new Li ion conducting pathways because of the interaction between constituents. The enhancement in term of mechanical properties after filler incorporation was also observed by Yap et al. [12] and this is due to the improved electrode-electrolyte stability. To our knowledge, this study is the first to use silica extracted from RHA in PMMA/ENR 50-based electrolyte system.

This work used the precipitation process to recover natural inorganic silica from RHA [13]. The extracted silica was analyzed for particle structure, size, phase, purity and morphology using Fourier transform infrared spectroscopy (FTIR), particle size analyzer (PSA), x-ray diffraction (XRD), energy dispersive x-ray spectroscopy (EDX) and scanning electron microscopy (SEM) techniques, respectively. The PMMA/ENR50 films were prepared with varying concentrations of silica (0.25, 0.5, 0.75, and 1.0 wt. %). The solution casting method was chosen owing to its simplicity [5]. The electrical characteristics of the polymer electrolyte for silica-doped PMMA/ENR 50 were investigated using the electrochemical impedance spectroscopy (EIS) while FTIR analysis indicates the structural behaviors of the electrolyte films.

EXPERIMENTAL

Chemicals and Materials

ENR 50 was acquired from Lembaga Getah Malaysia (LGM), whereas the RHA was obtained from the rice mill in Perlis. PMMA (molecular weight: 120,000 g/mol), tetrahydrofuran (THF), sodium hydroxide (NaOH) and lithium triflate (LiTf) with purity of 99.995 % were purchased from Merck (Darmstadt, Germany). Other chemicals such as sulfuric acid (98% H_2SO_4) and hydrochloric acid (37% HCl) were obtained from Fisher Scientific (Massachusetts, United States). No further purification was required for all chemicals used.

Extraction of Silica from RHA

The work of Farhan & Ebrahim [13] was referred for the silica extraction process. In order to eliminate contaminants, 20 g of RHA was first treated with 120 mL of 2 N HCl (**Figure 1(a)**) at 80 °C for 2.5 hours. After that, it was kept at room temperature for 12 hours. The mixture was dried at 105 °C for 5 hours after being filtered (**Figure 1(b)**) and rinsed with hot distilled water until the pH reached 5.5. Next, the dried RHA was burned for five hours at 700 °C in a furnace to produce pure white silica powder. Sodium silicate was created (**Figure 1(c)**) by combining 10 g of this powder with 80 mL of 2.5 N NaOH at 95 °C for 3 hours in order to create silica gel. After filtering the mixture (**Figure 1(d)**) and adding H_2SO_4 to precipitate the silica gel (**Figure 1(e)**), the mixture was cleaned until the pH reached a neutral value. White silica powder was created by drying the resultant silica at 100 °C for 12 hours (**Figure 1(f)**). Equation (1) was used to calculate the percentage yield of silica [14].

$$\text{Percentage yield of silica (\%)} = \frac{\text{Mass of produced silica (g)}}{\text{Mass of RHA (g)}} \times 100\% \quad (1)$$

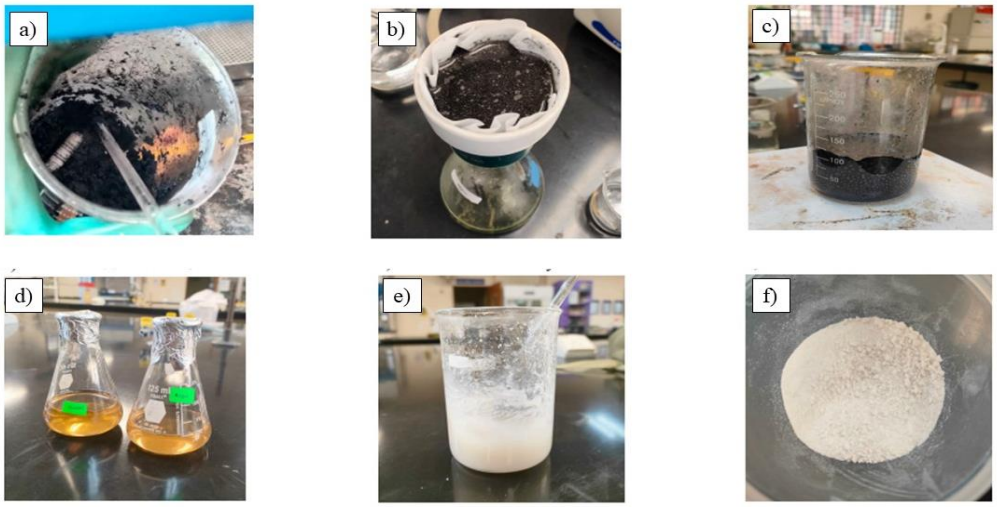

Figure 1. Schematic diagram for the extraction of silica.

Preparation of Electrolyte Based on Silica-doped PMMA/ENR 50

The solution casting technique was employed to prepare silica-doped PMMA/ENR 50-based electrolyte films [11]. Initially, PMMA, LiTf, ENR 50, and silica were each dissolved in tetrahydrofuran (THF) over a 24-hour period using a magnetic stirrer. Subsequently, varying amounts of silica were incorporated into the PMMA/ENR50/LiTf mixtures, which were stirred continuously until a homogeneous solution was achieved, indicating complete dissolution. The concentrations of LiTf and ENR 50 were maintained at 40% and 10%, respectively, within the PMMA matrix, as this specific composition had previously been determined to yield the highest conductivity [15]. The resultant solutions were then poured into petri dishes and left to dry in a fume hood for 24 hours. After drying, each film was stored in a desiccator prior to further characterization. Systems containing varying silica weight percentages were designated as $PMMAENR_0$ (0 wt.%), $PMMAENR_{0.25}$ (0.25 wt.%), $PMMAENR_{0.5}$ (0.50 wt.%), $PMMAENR_{0.75}$ (0.75 wt.%), and $PMMAENR_1$ (1.0 wt.%). Additionally, a blank PMMA/ENR50 film, labeled PMMAENR50, was prepared as a control.

Characterization Methods

Particle Size Analyzer (PSA)

PSA (MALVERN/MS2000) was utilized to determine the size of the particle of RHA extracted silica. PSA employs dynamic or infrared scattering technique which can detect Brownian motion in samples, resulting in a particle size of 0.1 nm to 10 μm.

Fourier-transform Infrared Spectroscopy (FTIR)

The RHA silica functional groups and the interaction of constituents in silica-doped PMMA/ENR 50 were identified using a Perkin Elmer Attenuated Total Reflectance (ATR)-FTIR spectroscopy. A frequency range of 4000 to 600 cm^{-1}, at a resolution of 2 cm^{-1} with 16 scans were used to collect the data.

X-Ray Diffraction Analysis (XRD)

The phase of RHA and the extracted silica was investigated using XRD (RIGAKU/XRD D/MAX 2200V/PC). The 2θ diffraction angle range of 10° to 60° was scanned at a rate of 10 per minute.

Scanning Electron Microscopy (SEM)- Energy Dispersive X-ray Spectroscopy (EDX)

The RHA morphology and extracted silica were obtained by using SEM (JEOL JSM-6380A Analytical SEM) at 5000x magnifications. In order to determine the elemental composition of the extracted silica and RHA, an EDX analysis was performed. Prior to measurement, the samples were coated with platinum using JFC-1600 auto fine coaters. Platinum has great electrical conductivity, which makes it ideal for effectively dissipating charge generated during SEM imaging.

Electrochemical Impedance Spectroscopy (EIS)

Using EIS (HIOKI 35232-01 LCR), the ionic conductivities of the electrolyte films based on silica-doped PMMA/ENR50 were ascertained. First, a micrometre screw gauge was used to measure the film's thickness. After that, the film was sandwiched between two electrodes composed of stainless steel. The impedance at room temperature was measured in the range of frequencies 100 Hz to 1 MHz, at three different points of the film. The ionic conductivity (σ) of the sample was calculated using Equation (2) subsequent to the determination of the bulk resistance (R_b) from the impedance plots.

$$\sigma = \frac{l}{R_b \cdot A} \quad (2)$$

where the film thickness, l in cm, the bulk resistance, R_b in Ω, and effective contact area between electrode and electrolyte, A in cm^2.

RESULTS AND DISCUSSION

Silica Extraction from RHA

The successful precipitation method of extracting white powdered silica from RHA is depicted in **Figure 1(f).** The percentage yield calculated was 48.59%. The methods of purification employed to get rid of impurities from the extracted silica that might affect total yield. Extended and more thorough purification procedure may induce loss in silica, resulting in a lower yield.

Characterizations of Silica

Particle Size Analysis of Silica

Figure 2 displays the distribution of size of the particle of extracted silica range 0.02 -206.50 μm, which had a mean particle size of 75.76 μm. The size of particle obtained was about similar to the result reported by A'yuni et al. [16] (81.20 μm), when extracting ultrafine silica from RHA using the sol-gel technique.

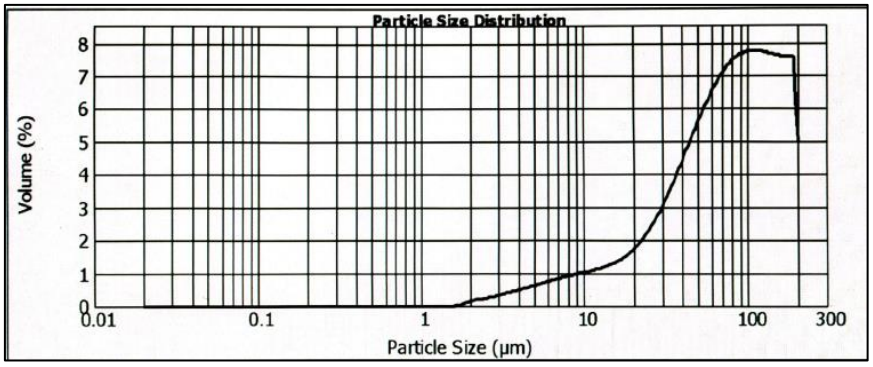

Figure 2. The size distribution of silica particles extracted from RHA.

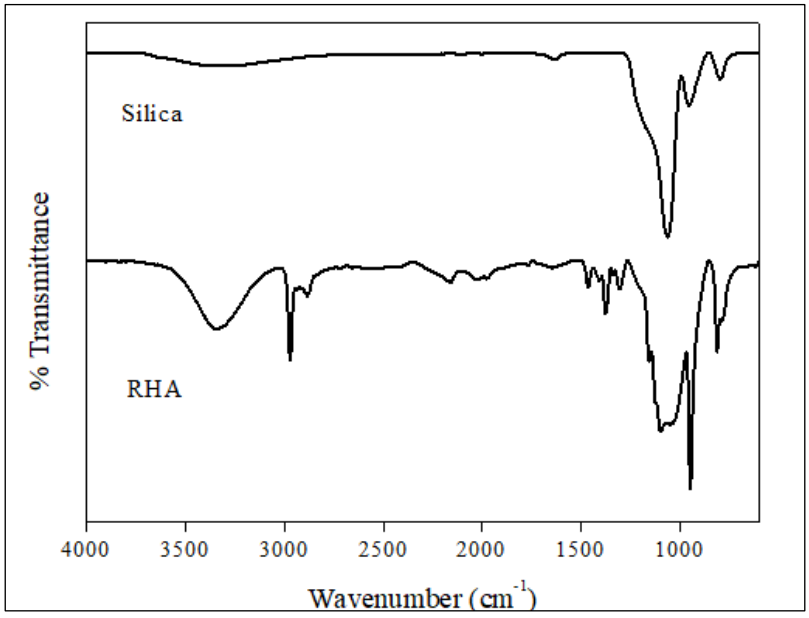

Figure 3. FTIR spectra of the extracted silica and RHA.

Structural Analysis of Silica

Figure 3 displays the FTIR spectra for extracted silica and RHA. The spectral peaks of RHA showed at 3339 cm^{-1}, ~2000 cm^{-1}, 1098 cm^{-1} and 814 cm^{-1} representing the stretching of Si−OH, CH, Si-O-Si and Si-O, respectively. Meanwhile the peak appeared at 1635 cm^{-1} referring to Si-OH bending. The extracted silica exhibited FTIR peaks at 3347 cm^{-1}, 1064 cm^{-1}, and 798 cm^{-1}, representing the stretching of Si-OH, Si-O-Si, and Si-O, respectively. Other peak that also can be observed at 1633 cm^{-1} represents the bending of Si-OH. Hu & Hsieh [17] and Thuadaij & Nuntiya [18] also reported the same peaks appeared for the silica from RHA. Hence, this proved that the precipitation technique has effectively extracted the silica from RHA. The FTIR spectra of silica showed no CH stretching peak. The disappearance of carbon generated during rice husk combustion hence confirms the purity of the silica.

Phase Analysis of Silica

Figure 4 displays the XRD diffractograms for the extracted silica and RHA. The RHA sample shows sharp peaks at 2θ angles of 22°, 38° and 44° on XRD diffractogram, indicating silica crystalline peaks. Zou & Yang [19] also reported the same insight. Meanwhile, the XRD diffractogram of silica shows a wide peak at 2θ angle of 24°, which denotes to the silica with amorphous nature. Research conducted by Ajeel et al. [20] and Kasinathan et al. [21] also supported this observation.

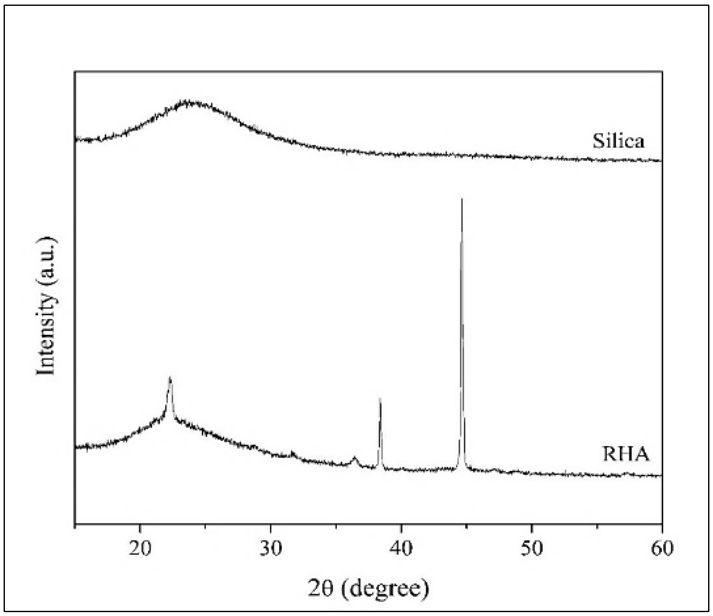

Figure 4. XRD diffractogram of extracted silica and RHA.

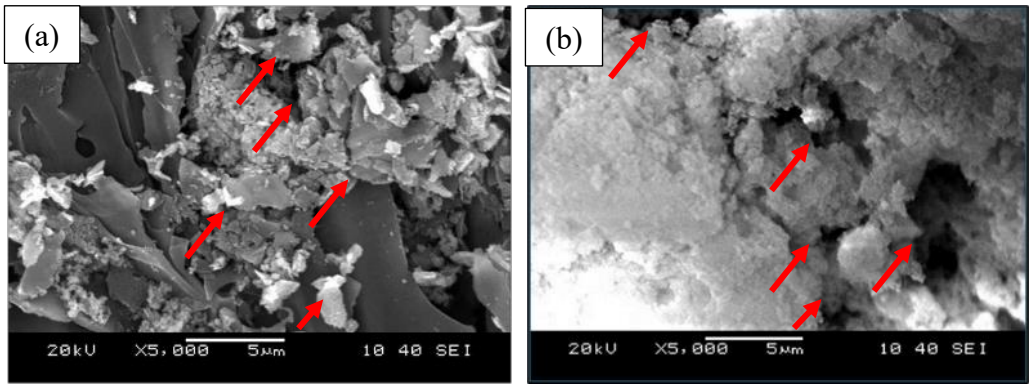

Figure 5. The morphologies surface of (a) RHA sample and (b) extracted silica.

EM-EDX Analysis of Silica

The surfaces morphologies of extracted silica and RHA were shown in **Figure 5**. **Figure 5(a)** indicates the image on SEM for RHA sample that shows larger fragments in the form of flake or plate-like agglomerates with small particles, verifying the existence of produced ash particles during combustion. The larger particles might be remnants (as indicated by the arrows) of the original structure of rice husk that did not completely break down throughout the process of combustion. Thus, the crystalline phase of RHA shown by the XRD analysis is further supported by the flake seen in the SEM image. As confirmed by the XRD study, the image of SEM produced from the silica that has been extracted (**Figure 5(b)**) demonstrates a porous (as indicated by the arrows) and agglomerated structure with uniform distribution within particle, indicating its amorphous nature. Kasinathan et al. [21] also observed similar findings for the RHA and the extracted silica.

Table 1 lists the elemental composition of RHA and the silica that was obtained from the EDX analysis. The elements present in RHA comprises of C, Si, O and K. This incomplete combustion of RHA resulted in a significant proportion of C which is 48.12 wt.%. As for the extracted silica, it contains solely Si and O. The absence of C and any other elements suggests that there are no contaminants in the extracted silica [13].

Table 1. The elemental composition in weight percentage of RHA and extracted silica.

Elements	RHA (wt. %)	Extracted silica (wt. %)
C	48.12	ND
O	29.42	40.44
Si	20.81	59.56
K	1.66	ND
Total	100.00	100.00

*ND: not detected

The Electrolyte Films Formation of Silica-doped PMMA/ENR 50

The film formed for PMMA/ENR50 (PMMAENR) was flexible, phase separated and opaque, as shown in **Figure 6(a)**. The elastomeric characteristics in ENR 50 contribute to the flexibility of the film. $PMMAENR_0$ (**Figure 6(b)**) displayed a more flexible and clearer phase separated film. Meanwhile, when 0.25 and 0.5 wt. % of silica were added to the PMMA/ ENR50-based electrolyte system, films with clear, flexible and without phase separation were successfully formed, as depicted in **Figure 6(c)** and **Figure 6(d)**, respectively. This might be resulted by the movement of ENR50 into the PMMA phase as the inorganic filler occupied the space between PMMA and ENR50. The same observation on the PMMA/ENR50-based films were also reported by Habep et al. [11] who used Al_2O_3 and Zamri et al. [5] who used commercial SiO_2. Habep et al. [11] suggested that no presence of phase separation can be attributed to the dipole-dipole interactions between polymer and filler. But after adding 0.75 weight percentage of silica, the films formed were sticky as shown in **Figure 6(e)**. Meanwhile, **Figure 6(f)** shows that upon the addition of 1 wt. % of silica, the film obtained were sticky as well as exhibiting phase separation. This proved that increment of weight percentage of silica enhanced the adhesiveness of the films. The film remained phase separated despite with the addition of highest weight percentage ($PMMAENR_1$) of silica which Basri et al. [4] also had same observation. This might be due to the congestion that occurred due to the excessive amount of silica.

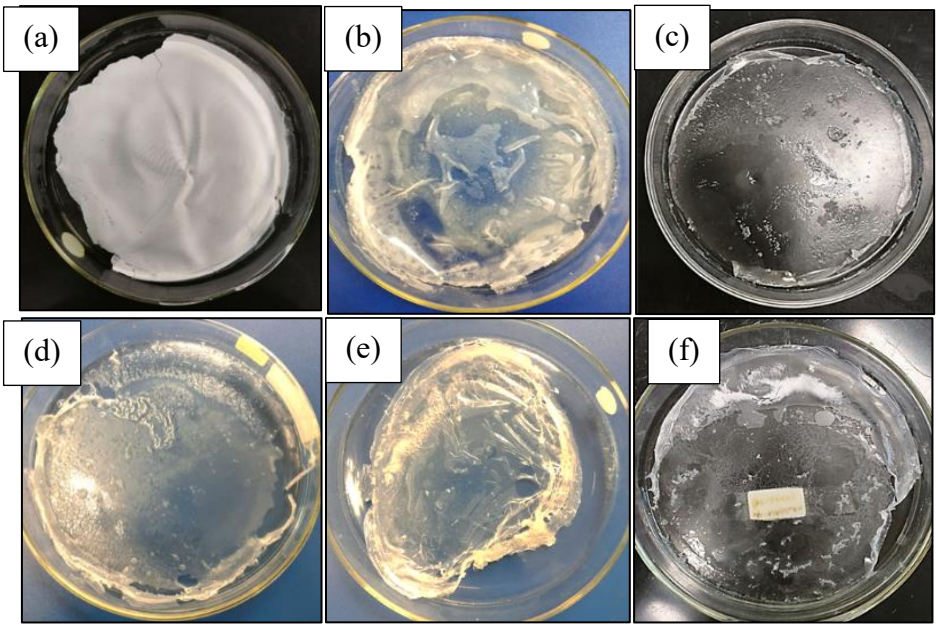

Figure 6. The (a) PMMAENR, (b) $PMMAENR_0$, (c) $PMMAENR_{0.25}$, (d) $PMMAENR_{0.5}$, (e) $PMMAENR_{0.75}$, and (f) $PMMAENR_1$ based electrolyte films.

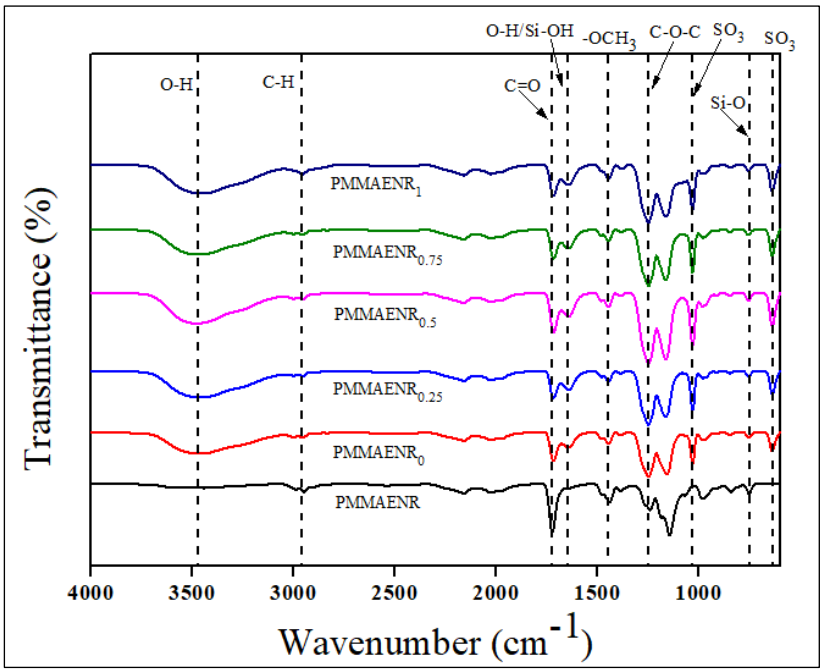

Figure 7. FTIR spectra for samples PMMAENR, $PMMAENR_0$, $PMMAENR_{0.25}$, $PMMAENR_{0.5}$, $PMMAENR_{0.75}$ and $PMMAENR_1$ based electrolyte system.

Characterizations of Electrolyte Films of Silica-doped PMMA/ENR 50

Structural Analysis of Electrolyte Based on Silica-doped PMMA/ENR 50

Figure 7 displays the FTIR spectra results obtained for all the samples ($PMMAENR_0$ and $PMMAENR_{0.25-1}$). The peaks representing PMMAENR were seen at 3468 cm^{-1} and 2955 cm^{-1} that represents O-H and C-H stretching, while peaks at 1724 cm^{-1}, 1441 cm^{-1} and 1241 cm^{-1}, attributing to the stretching of C=O, $-OCH_3$ and C-O-C, respectively. The appearance of the OH stretching peak was resulted from the interaction of hydrogen bonding between polymers, which similar with previous observations done by Zamri et al. [5] and Habep et al. [11].

Upon the addition of LiTf into the PMMA/ ENR 50 mix system, the additional peaks at 1032 cm^{-1} and 639 cm^{-1} were discovered that indicate SO_3 stretching and SO_3 bending, respectively. These peaks indicate that the LiTf was effectively absorbed into the blend system, same as observed by Syafiq et al. [22]. The stretching peak of C=O for PMMA at 1724 cm^{-1} was shifted to 1718 cm^{-1} and the peak intensity also decreased, which indicating the influence of the addition of LiTf. In addition, the $-OCH_3$ stretching increase in wavenumber from 1441 cm^{-1} and changed to 1446 cm^{-1}, with decrease in peak intensity. The stretching peak of C-O-C for ENR50 sample which was previously seen at 1241 cm^{-1} wavenumber was changed to 1249 cm^{-1} with the increment of peak intensity. The results obtained indicated the interaction was occurred between the salt of lithium cations and an atom of oxygen for PMMA/ENR 50 sample, as Zamri et al. [5] also reported the same finding. The addition of LiTf was also shown to broaden the stretching peak of OH, suggesting the hygroscopic nature of LiTf implies the presence of moisture. This has been verified by the presence of a water OH bending peak at 1664 cm^{-1}.

The addition of silica resulted in new peak at ~ 1646 cm^{-1} represent the bending of Si-OH and peak at ~ 750 cm^{-1} refers to the stretching of Si-O. Hu & Hsieh [17] also reported similar results as the absorption bands obtained, which shows the silica was successfully incorporated in the system. It also can be seen that the wavenumbers for stretching peaks of C=O, C-O-C and $-OCH_3$ remained unchanged. However, for C=O and $-OCH_3$ peaks shows the decrease in peak intensity, whereas C-O-C peak increased with the addition 0.25, 0.5, 0.75 and 1.0 wt. % of silica into the system, which confirmed the interaction between polymer and filler. As shown in **Figure 7**, both SO_3 bending and SO_3 stretching peak shows an unchanged wavenumbers results, with increase in peak intensities. This verified the interaction occurred between salt and fillers. Habep et al. [11] stated that the amorphous phase of the electrolyte will be improved by the interaction of polymer, salt and filler of the system.

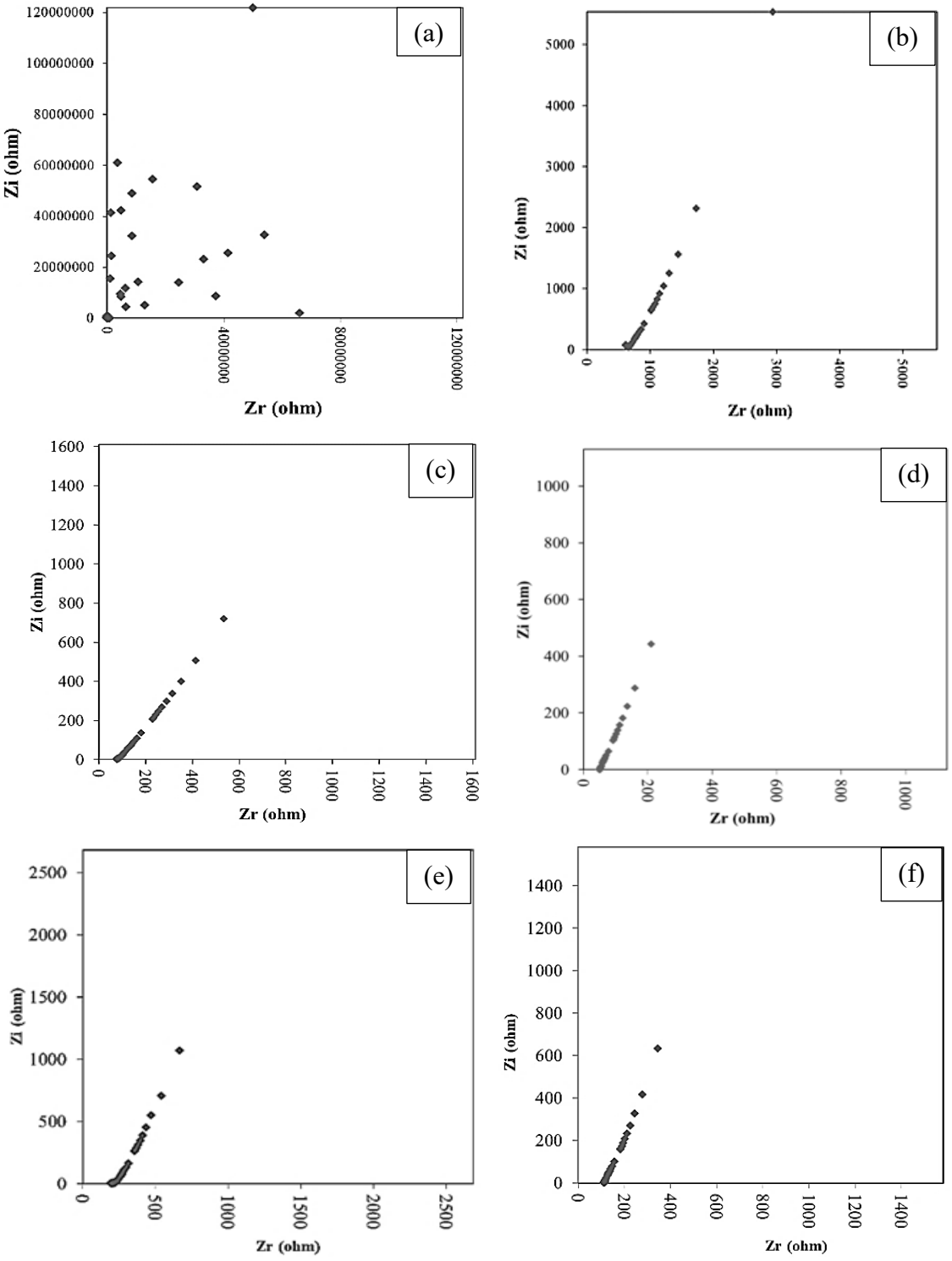

Figure 8. Cole-Cole plots of (a) PMMAENR, (b) $PMMAENR_0$, (c) $PMMAENR_{0.25}$, (d) $PMMAENR_{0.5}$, (e) $PMMAENR_{0.75}$ and (f) $PMMAENR_1$ based electrolyte samples.

Electrochemical Analysis Electrolyte Films of Silica-doped PMMA/ENR 50

Figure 8(a) showed the Cole-Cole plot of PMMAENR which exhibited a scattered result. Šoljić et al. [23] stated that many sources of interference contributed to this scattered result which interfered with the coating impedance measurement. Meanwhile, the semicircle and spike can be seen on $PMMAENR_0$ sample in **Figure 8(b)**. According to Habep et al. [11], the polymer electrolyte's bulk conductance, or the parallel sum of R_b, and its bulk capacitance were shown via the formation of a semicircle. Bulk resistance is caused by mobile ions in the matrix, whereas the bulk capacitance is often produced by stiff polymer chains. **Figure 8(c)-(f)**

displayed the Cole-Cole plots for $PMMAENR_{0.25-1}$ which denotes new spikes appeared due to the interface charge transfer, resulting in double layer capacitance. Furthermore, the diffusion of ion existence can be confirmed by the spike result obtained from the sample [24].

The ionic conductivities were computed by using Equation (2), as for R_b was taken from the Cole-Cole plots. The results of ionic conductivity of silica-doped PMMA/ENR50-based electrolyte films samples were listed in **Table 2**.

The PMMAENR film shows the σ of 1.09×10^{-9} S/cm. With the addition of LiTf, the conductivity then enhanced to 7.29×10^{-5} S/cm. This was attributed to the charge carrier mobility that consisted of Li^+ ions present in the system, as observed and reported by Habep et al. [11].

After the incorporation of 0.25 wt. % of silica in the system, its σ enhanced to 7.19×10^{-4} S/cm and continued to increase when 0.5 wt. % of silica added which gave σ of 1.37×10^{-3} S/cm. FTIR analysis confirms that polymer-filler interactions contributed to the increment of amorphicity of the system which led to the increase of σ. The enhanced ionic conductivity with filler inclusion can be explained by the amorphous phase enhancement of mobility of Li^+ ions. The interaction between filler and salt was validated by the FTIR study, opening up novel conducting routes for Li^+ ions. Thus, in accordance with a research by Habep et al. [11], this improves ionic transit in the polymer electrolyte. Meanwhile, σ gradually decreased as the silica level was raised over 0.5 wt. %. This is probably due to the system being clogged with a presence of large amount of concentration in silica [25].

In other words, as the silica particles in the polymer came closer together, they began to agglomerate and creating obstacles effects. Previous studies had shown that this congestion restricts polymer chain movement, which in turn reduces the ionic conductivity [4]. Dennis et al. [26] also noted the same observation, stating that the addition of 10 wt. % ZnO nanofillers reduced the ionic conductivity in nanocomposite solid polymer electrolytes (NCSPEs).

Table 3 lists the different results of ionic conductivities study from other silica-doped PMMA-based blend electrolyte system. From the table, an ionic conductivity obtained in this study (~10^{-3} S/cm) is higher if compared with other systems (~10^{-6} S/cm) listed. The lower silica content used in this study was contributed to this improvement. This was probably caused due to the large amount of silica presence which make the system being clogged [27]. Other than that, it was observed that the system incorporated with macron-sized silica in this study is more conducting if compared to the nano-sized commercial silica used in other studies. This happened as the result of blocking effect due to the tendency of nano-sized silica grains to get closer to each other. The same observation was reported by Yap et al. [12] who compared the performance of micron and nano-sized filler (silica and alumina) in the poly(ethylene oxide) (PEO)- based electrolyte system.

Table 2. The ionic conductivity of electrolyte based on silica-doped PMMA/ENR50.

Sample	R_b (Ω)	Conductivity (S/cm)
PMMAENR	6.50×10^7	$1.09 \pm 0.66 \times 10^{-9}$
$PMMAENR_0$	6.85×10^2	$7.29 \pm 3.48 \times 10^{-5}$
$PMMAENR_{0.25}$	9.78×10^1	$7.19 \pm 1.81 \times 10^{-4}$
$PMMAENR_{0.5}$	5.32×10^1	$1.37 \pm 0.17 \times 10^{-3}$
$PMMAENR_{0.75}$	2.35×10^2	$5.15 \pm 1.40 \times 10^{-4}$
$PMMAENR_1$	1.18×10^2	$7.18 \pm 0.50 \times 10^{-4}$

Table 3. Ionic conductivities of other silica-doped PMMA-based blend electrolyte system.

Polymer System	Weight Percentage of SiO_2 (wt.%)	Size of filler	Conductivity (S/cm)	Reference(s)
PMMA/ENR50/LiTf	0.5	75.76 μm	1.37×10^{-3}	This study
PMMA/ENR 50/$LiBF_4$	3.0	20.00 nm	1.80×10^{-6}	[25]
PMMA/ ENR50/$LiBF_4$	5.0	15.00 nm	5.30×10^{-6}	[28]
PMMA/PEG/$LiBF_4$	3.0	15.00 nm	5.55×10^{-6}	[4]

CONCLUSION

The addition of 0.5 wt.% of silica to electrolyte system of PMMA/ENR 50 resulted in flexible, homogeneous and free-standing films with the highest conductivity of 1.37×10^{-3} S/cm. This was explained by the development of a new Li ion conducting channel that was brought about by the interaction of the filler and salt, as well as an increase in the amorphous phase of the system caused by the polymer-filler interaction. This system shows potential in lithium-ion batteries application due to its excellent conductivity result. Further work should be continued related to thermal and mechanical characteristics of the system to ensure the successful implementation of energy storage devices application.

ACKNOWLEDGEMENTS

The Ministry of Higher Education discloses support for this work through Fundamental Research Grant Scheme (Grant No. FRGS/1/2023/STG05/UITM/02/13). The authors would also like to extend their sincere gratitude to the Faculty of Applied Sciences, Universiti Teknologi MARA (UiTM) Shah Alam and Perlis branch for their support of this research.

REFERENCES

1. Chen, Y., Kang, Y., Zhao, Y., Wang, L., Liu, J., Li, Y., Liang, Z., He, X., Li, X., Tavajohi, N. and Li, B. (2021) A review of lithium-ion battery safety concerns: The issues, strategies, and testing standards. *Journal of Energy Chemistry*, **59**, 83–99.

2. Ngai, K. S., Ramesh, S., Ramesh, K. and Juan, J. C. (2016) A review of polymer electrolytes: fundamental, approaches and applications. *Ionics*, **22(8)**, 1259–1279.

3. Latif, F. A., Zailani, N. A. M., Shukaili, Z. S. M. A., Zamri, S. F. M., Kasim, N. A. M., Rani, M. S. A. and Norrahim, M. N. F. (2022) Review of poly (methyl methacrylate) based polymer electrolytes in solid-state supercapacitors. *International Journal of Electrochemical Science*, **17(1)**, 22013.

4. Basri, N. D., Latif, F., Ibrahim, R., Susila, F., Ghani, A., Fadli, S. and Zamri, M. (2021) Formation, Morphological, Molecular Interaction and Ionic Conductivity of SiO_2 Filled PMMA/ PEG Electrolytes. *Malaysian Journal of Analytical Sciences*, **25**, 234–242.

5. Zamri, S. F. M., Latif, F. A., Ali, A. M. M., Ibrahim, R., Azuan, S. I. H. M., Kamaluddin, N. and Hadip, F. (2018) Filler and polymer interactions in polymethyl methacrylate/50% epoxidized natural rubber/silicon dioxide nanocomposites. *Malaysian Journal of Analytical Sciences*, **22(4)**, 586–593.

6. Harun, F. and Chan, C. H. (2016) Electronic applications of polymer electrolytes of epoxidized natural rubber and its composites. *Flexible and Stretchable Electronic Composites*, 37–59.

7. Sionkowska, A. (2023) Current research on the blends of natural and synthetic polymers as new biomaterials: Review. *Progress in Polymer Science*, **36(9)**, 1254–1276.

8. Yazie, N., Worku, D., Gabbiye, N., Alemayehu, A., Getahun, Z. & Dagnew, M. (2023) Development of polymer blend electrolytes for battery systems: recent progress, challenges, and future outlook. *Materials for Renewable and Sustainable Energy*, **12(2)**, 73–94.

9. Yang, X., Liu, J., Pei, N., Chen, Z., Li, R., Fu, L., Zhang, P. and Zhao, J. (2023) The critical role of fillers in composite polymer electrolytes for lithium battery. *Nano-Micro Letters*, **15(1)**, 2–37.

10. Dissanayake, M. A. K. L., Rupasinghe, W. N. S., Jayasundara, J. M. N. I., Ekanayake, P., Bandara, T. M. W. J., Thalawala, S. N. and Seneviratne, V. A. (2013) Ionic conductivity enhancement in the solid polymer electrolyte PEO9LiTf by nanosilica filler from rice husk ash. *Journal of Solid-State Electrochemistry*, **17(6)**, 1775–1783.

11. Habep, N. A., Zailani, N. A. M., Zaharuddin, I. Q., Nazir, K., Muhammad, F. H., Yahya, S., Ghani, F. S. A., and Latif, F. A. (2023) Effect of nanoalumina (Al_2O_3) filler on the properties of poly(methyl methacrylate) (PMMA)/50% epoxidized natural rubber (ENR 50) electrolytes. *Malaysian Journal of Chemistry*, **25(4)**, 222–231.

12. Yap, Y. L., You, A. H., Teo, L. L. & Hanapei, H. J. I. J. E. S. (2013) Inorganic filler sizes effect on ionic conductivity in polyethylene oxide (PEO) composite polymer electrolyte. *International Journal of Electrochemical Science*, **8(2)**, 2154-2163.

13. Farhan, R. Z. and Ebrahim, S. E. (2021) Preparing nanosilica particles from rice husk using precipitation method. *Baghdad Science Journal*, **18(3)**, 494–500.

14. Nayak, P. P. and Datta, A. K. (2021) Synthesis of SiO_2-nanoparticles from rice husk ash and its comparison with commercial amorphous silica through material characterization. *Silicon*, **13(4)**, 1209–1214.

15. Latif, F., Aziz, M., Katun, N., Ali, A. M. M. and Yahya, M. Z. (2006) The role and impact of rubber in poly (methyl methacrylate)/lithium triflate electrolyte. *Journal of Power Sources*, **159(2),** 1401–1404.

16. A'yuni, D. Q., Djaeni, M., and Subagio, A. (2021) Characterization of ultrafine silica prepared from rice husk ash by sol-gel method. *Conference Series: Materials Science and Engineering*, **1053(1)**, 012072.

17. Hu, S. and Hsieh, Y. Lo. (2014) Preparation of activated carbon and silica particles from rice straw. *ACS Sustainable Chemistry and Engineering*, **2(4)**, 726–734.

18. Thuadaij, N. and Nuntiya, A. (2008) Preparation of nanosilica powder from rice husk ash by precipitation method. *Chiang Mai Journal of Science*, **35(1)**, 206–211.

19. Zou, Y. and Yang, T. (2019) Rice husk, rice husk ash and their applications. In Rice bran and rice bran oil. *AOCS Press*, 207–246.

20. Ajeel, S. A., Sukkar, K. A. and Zedin, N. K. (2020) Extraction of high purity amorphous silica from rice husk by chemical process. *IOP Conference Series: Materials Science and Engineering*, **881(1)**.

21. Kasinathan, A., Rama, R. and Sivakumar, G. (2010) Extraction, synthesis, and characterization of nanosilica from rice husk ash. *International Journal of Nanotechnology and Applications*, **4**, 61–66.

22. Syafiq, A., Asnawi, F., Amalina, A., Azli, M., Hafiz Hamsan, M., Fakhrul, M., Kadir, Z. and Yusof, Y. (2020) Electrical and infrared spectroscopic analysis of solid polymer electrolyte based on polyethylene oxide and graphene oxide blend. *Malaysian Journal of Analytical Sciences*, **24**, 682–697.

23. Šoljić, I., Šoić, I., Kostelac, L. and Martinez, S. (2022) AC interference impact on EIS assessment of organic coatings using dummy cells, calibration foils and field exposed coated samples. *Progress in organic coatings*, **165**, 106767.

24. Tang, W., Tang, S., Zhang, C., Ma, Q., Xiang, Q., Yang, Y. W. and Luo, J. (2018) Simultaneously enhancing the thermal stability, mechanical modulus, and electrochemical performance of solid polymer electrolytes by incorporating 2D sheets. *Advanced Energy Materials*, **8(24)**.

25. Zamri, S. F. M. and Latif, F. A. (2013) SiO_2 filler as interface modifier in PMMA/ENR 50 electrolytes. *Advanced Materials Research*, **812**, 120–124.

26. Dennis, J. O., Adam, A. A., Ali, M. K. M., Soleimani, H., Shukur, M. F. B. A., Ibnaouf, K. H., Aldaghri, O., Eisa, M. H., Ibrahem, M. A., Abdulkadir, A. B. and Cyriac, V. (2022) Substantial proton ion conduction in methylcellulose/pectin/ ammonium chloride based solid nanocomposite polymer electrolytes: Effect of ZnO nanofiller. *Membranes*, **12(7)**, 706.

27. Ahmad, A., Rahman, M. Y. A., Low, S. P. & Hamzah, H. (2011) Effect of $LiBF_4$ Salt Concentration on the Properties of Plasticized MG49-TiO_2 Based Nanocomposite Polymer Electrolyte. *International Scholarly Research Notices*, **2011(1)**, 401280.

28. Zamri, S. F. M., Latif, F. A., Ali, A. M. M., Ibrahim, R., Azuan, S. I. H. M., Kamaluddin, N. and Hadip, F. (2017) Exploration on effects of 15 nm SiO_2 filler on miscibility, thermal stability, and ionic conductivity of PMMA/ENR 50 electrolytes. *AIP Conference Proceedings*, **1809**.